Arch. Min. Sci. **70** (2025), 4, 625-641

Electronic version (in color) of this paper is available: http://mining.archives.pl

DOI: https://doi.org/10.24425/ams.2025.157451

BAOLIN LI[1], JIE SONG[1*], WENBO GUAN[2],
ZHANKAI WU[3], ZENGRONG ZHENG[4]

A STUDY ON FRACTAL ANALYSIS OF PORE STRUCTURES IN COAL SEAMS: IMPLICATIONS FOR GAS EXPANSION ENERGY AND METHANE RECOVERY

Methane, the primary component of coalbed methane (CBM), plays a crucial role in reducing greenhouse gas emissions and mitigating coal mine safety risks. However, the efficient extraction of CBM is hindered by the complexity of coal seam pore structure (CSPS). This study investigates the impact of pore structure on methane gas expansion energy recovery using an intelligent operation coal mine in Province G, China, as a case study. Fractal theory was employed to analyse coal seam pore structure, and experimental results revealed that the microporous pore volume percentage in coal samples from two mines exceeded 85%, with a mean microporous specific surface area (SSA) percentage of 98.20% and 95.75%, respectively. A direct correlation was observed between increasing SSA and enhanced methane adsorption capacity. Additionally, a positive relationship was found between coal sample fractal dimension (FD) and methane adsorption, indicating that a more intricate pore structure enhances methane retention.

The findings suggest that optimising coal seam pore structure can significantly improve methane recovery efficiency, thereby reducing the risk of coal mine accidents and enhancing safety measures. By elucidating the role of CSPS in methane recovery, this study provides a scientific foundation for improving gas expansion energy recovery, particularly for methane extraction.

Keywords: Coal seam pore structure; Fractal theory; Methane recovery; Adsorption; Langmuir modelling

[1] ZHEJIANG UNIVERSITY OF WATER RESOURCES AND ELECTRIC POWER, COLLEGE OF CIVIL ENGINEERING AND ARCHITECTURE, HANGZHOU 310000, CHINA
[2] CHONGQING RESEARCH INSTITUTE, CHINA COAL TECHNOLOGY ENGINEERING GROUP, CHONGQING 400037, CHINA
[3] HANGZHOU RUHR TECHNOLOGY LTD, HANGZHOU 310000, CHINA
[4] DI-MATRIX (SHANGHAI) INFORMATION TECHNOLOGY CO., LTD, SHANGHAI, 200000, CHINA
* Corresponding author:zdbz520@163.com

1. Introduction

With the growing global energy demand and increasing awareness of environmental protection, the development and utilisation of coalbed methane (CBM) as a clean energy source has received widespread attention. Methane, one of the main components of CBM, can be efficiently recovered to reduce greenhouse gas emissions and mitigate the risk of coal mine safety accidents [1]. However, the effective extraction of CBM faces technical challenges, particularly due to the complexity of the coal seam pore structure (CSPS), which significantly affects methane adsorption (MAD), storage, and transport properties [2,3].

Relevant studies have shown that as coal seam tectonics intensify, the total pore volume (PV) of the coal increases, leading to a greater specific surface area (SSA). This contributes to a higher degree of media fragmentation, enhanced CBM adsorption capacity, and a greater risk to coal mine safety [4,5]. Consequently, it is crucial to examine how CSPS affects methane expansion energy and to investigate CSPS in detail.

The effects of CSPS on methane recovery have received less attention in current studies compared to coal metamorphism, temperature, pressure, and SSA [6]. To address this gap, this study conducts a fractal analysis of CSPS, using an intelligent operation coal mine in Province G, China, as a case study. The effect of CS pores on methane gas expansion energy recovery (desorption and adsorption) is further explored. This study aims to clarify the role of CSPS in methane expansion energy recovery and other coal seam gases, reduce coal mine safety risks, and improve the efficiency of safe coal mining.

2. Literature review

Coal rock bodies contain abundant pores, which serve as the primary storage sites for methane and other CBM gases, as well as the main channels for gas expansion energy diffusion and movement. Analysing the pore structure (PS) of coal rock bodies is therefore of significant importance for the mining and utilisation of methane and other CBM gases.

Ma D. et al. [7] proposed a testing device and method for analysing fractured rock bodies under coupled seepage and stress conditions to examine the mechanism of water damage in fault-broken zones during coal mining. Their technique evaluated the PS and permeability properties of the fractured rock body while controlling for stress and grain size distribution. The study indicated that the absence of small grain sizes led to an increase in porosity and maximum pore size (PSi) while reducing the compressibility of the fractured rock body specimen

To address the risk posed by high gas concentrations in middle- and high-order CSs during production, Yuan Y. et al. [8] developed a method to examine the PS characteristics of coal using low-temperature liquid nitrogen adsorption (NA)-desorption technology and the Kelvin equation. This method utilised scientific analysis methodologies and electron microscope (EM) scanning to accurately classify and evaluate the PS of coal samples (CSas)

Razavifar M. et al. [9] investigated the accuracy of PS characterisation in geological materials by combining conventional PS characterisation techniques such as mercury intrusion porosimetry (MIP), nuclear magnetic resonance (NMR), micro-X-ray computed tomography (CT) imaging, and gas injection. Their study compared porosity and permeability results obtained from different techniques and found that NMR predictions provided a better approximation of the PSi distribution obtained from micro-X-ray CT.

Li C. et al. [10] developed the liquid nitrogen freeze-thaw fracturing method to enhance the efficiency of low-permeability CSs in CBM production. This method not only increased CBM recovery but also improved the PS characteristics and permeability of middle- and high-order coals.

To clarify the structural transformations occurring during methane and propane flue gas substitution, as well as the guest molecule distribution pattern, Choi W. et al. [11] conducted structural observation and analysis using gas chromatography and NMR. The study employed a flue gas injection method to examine the replaced gas hydrates using powder X-ray diffraction, revealing that carbon dioxide (CO_2) and nitrogen compete to maintain hydrate stability.

Pandey J.S. et al. [12] analysed the dissociation behaviour of the methane/CO_2 hydrate system to enhance methane and CO_2 storage capacity. Their study used a multi-step cyclic depressurisation method to dissociate bulk methane/CO_2 hydrates, examining changes in methane and CO_2 morphology and molar fraction. The results indicated that water released from dissociation had a reforming effect on the hydrate.

Zhou Y. et al. [13]proposed a high-efficiency heat flow reversal reactor to address the thermal pollution problem caused by methane emissions from coal mine ventilation exhaust. Their study conducted a comparative analysis of five different heat extraction strategies, leading to efficient methane recovery and heat energy reuse.

To examine the effects of coal nanopore structure transformation induced by phase change fracturing of liquid CO_2, Liu G. et al. [14] analysed large-scale PS changes in coal and the impact on gas adsorption capacity using MIP, pore simulation methods, low-temperature NA, and isothermal adsorption. Their study proposed a novel liquid CO_2 phase change fracturing technique based on modifications in gas saturation and critical desorption pressure to enhance CBM recoverability.

Ali A.M. et al. [15] investigated the energy distribution mechanisms involved in methane gas adsorption in shale through simulations aimed at clarifying the possibility of MAD in shale under reservoir pressure conditions. Their study analysed the effect of pressure on MAD using atomic/molecular-level inputs.

Based on the above studies, it is evident that researchers have conducted extensive investigations into coal structure and the adsorption/desorption behaviour of gases such as methane. However, a significant experimental gap remains regarding the effect of coal seam internal pore structures on methane gas expansion energy recovery. Further research is needed to comprehensively explore the adsorption and desorption capabilities of CS structures and their impact on methane recovery.

Therefore, this study investigates CSPS and its influence on methane gas expansion energy using fractal theory, with an intelligent operation coal mine in Province G, China, as a case study. In addition to reducing the likelihood of unsafe airflow in coal mines, the study aims to elucidate the role of CS pores in methane recovery efficiency. What makes this investigation unique is its consideration of the structural pore properties of various CSas, along with tests and analyses conducted based on MAD and methane desorption (MDE) rates.

TABLE 1 summarises the commonly used techniques for pore structure analysis in coal, highlighting their applicable pore size ranges, resolution, and suitability for different analytical objectives. This comparison underscores the complementary nature of these methods, as no single technique can fully characterise the multiscale pore system relevant to CBM storage and migration.

TABLE1

Comparative Summary of Pore Structure Characterisation Techniques Used in Coal Studies

Technique	Pore Size Range	Resolution	Advantages	Limitations
MIP (Mercury Intrusion Porosimetry)	~3 nm to 100 μm	High (for meso/macro)	Fast, wide pore size range, high-pressure measurement	Cannot detect micropores; sample damage; assumes cylindrical pores
NA (N_2 Adsorption at 77 K)	~0.5 to 100 nm	High (esp. micropores)	Well-established, suitable for micropore and SSA analysis	Not suitable for macropores; low temp may underrepresent in-situ behaviour
CO_2 Adsorption (273 K)	~0.3 to 1.5 nm	Ultra-high	Effective for ultra-micropores <1 nm; reflects gas adsorption sites	Limited to very small pores; requires careful isotherm modelling
NMR (Low-field)	All pore sizes (effective porosity)	Moderate	Non-destructive, detects fluid saturation & pore connectivity	Needs calibration; can't resolve pore shape/ geometry well
CT (Micro/ Nano X-ray)	>1 μm (macro)	Moderate to high	3D visualisation, shape analysis, fracture mapping	Limited resolution for micropores; expensive
SAXS / SANS	1-100 nm	High (sub-nano)	Non-destructive, wide range, high accuracy	Needs specialised equipment; model-dependent interpretation

3. Materials and methods

This section begins by providing an overview of the research areas, Mining Area A (MA-A) and Mining Area B (MA-B). Next, a fractal permeability model for CSs is developed based on fractal theory, followed by an introduction to the instruments used in the experiments. Finally, MAD and MDE experiments are designed. All key measurements, including nitrogen adsorption-desorption isotherms, specific surface area (SSA), and pore volume (PV) determinations, were conducted in triplicate for each coal sample to ensure repeatability. The data presented in the tables and figures reflect the mean values obtained from these repeated measurements. The standard deviation for SSA was within ±1.2 m^2/g, and for micropore volume, it was within ±0.005 cm^3/g. Adsorption capacity (MAD) tests showed a repeatability within ±3.5% of the measured values. The nitrogen adsorption analyses were performed using a Quantachrome Autosorb iQ 2 analyser with an instrumental accuracy of ±1%. This level of consistency suggests that the observed differences in SSA, PV, and methane adsorption capacity between MA-A and MA-B are statistically significant and not due to random measurement error. These repeatability results strengthen the reliability of the comparative conclusions drawn in the study.

3.1. Overview of the coal mine

The study takes the MA-A and MA-B of intelligent operation coal mines in Province G, China, as the CSa collection area and research object. MA-A covers 35.92 km^2, with total coal

resources of 2.256 billion tons, resource reserves of 0.99 billion tons, recoverable reserves of 0.55 billion tons, a coal content coefficient of 9.9%, and an average CS thickness of 12.5 m.

MA-B covers 66.70 km^2, with recoverable reserves of 320 million tons, a coal content coefficient of 7.60%, and an average CS thickness of 295.36 m. Although both MA-A and MA-B are located within Province G and share a broadly similar sedimentary and tectonic setting, subtle differences in depositional environment, burial history, and structural evolution may contribute to variations in coal properties. The coals are primarily high-volatile bituminous in rank and are hosted within Permian coal-bearing sequences, typical of the region. However, due to the lack of detailed petrographic and metamorphic data, a comprehensive evaluation of lithotype and rank differences was not possible. Therefore, while the findings offer valuable insights into the relationship between pore structure and methane recovery in the studied region, caution should be exercised in generalising these results to other coalfields with differing geological, structural, or thermal maturity conditions. The tectonic layout of MA-A and MA-B is illustrated in Fig. 1.

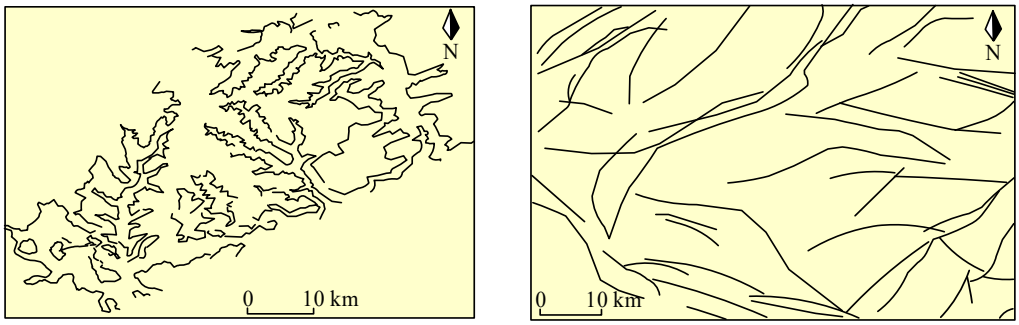

(a) Tectonic outline of the A mine shaft field (b) Tectonic outline of the B mine shaft field

Fig. 1. Outline map of the well field structure of the two MAs

As shown in Fig. 1(a), the main tectonic structure of MA-A consists of gently inclined folds of the next order. The stratigraphy generally trends northeast (NE), while the inclination is predominantly towards northwest (NW) and southeast (SE). The inclination angle ranges from 5° to 10°, indicating moderate tectonic complexity. In Fig. 1(b), MA-B exhibits a more folded structure. This study focuses on the structural analysis of No. 9 CS in MA-A and No. 20 CS in MA-B. The No. 9 CS in MA-A has an average thickness of 3.45 m and a recoverable rate of 100%. It is relatively stable in development, with a high methane and CBM content, leading to elevated intra-seam pressure and significant safety risks. The No. 20 CS in MA-B has an average thickness of 2.8 m and primarily consists of mudstone. Some sections contain siltstone mudstone, while the CS is primarily composed of crushed granular material, with relatively stable geological development. The methane content and intra-seam pressure of No. 9 CS in MA-A and No. 20 CS in MA-B are shown in TABLE 2.

In total, nine samples were analysed from each mining area, and the data in TABLE 2 represent the average values derived from these samples. As shown in TABLE 2, the methane content in No. 9 CS of MA-A is significantly higher, and the internal seam pressure is greater. In contrast, the highest methane content in No. 20 CS of MA-B reaches only 13.18 m^3/t. Its intra-seam gas expansion pressure is relatively low, resulting in poor permeability. Although the seams in MA-A

TABLE 2

Statistics of methane content and intra-layer pressure in the A and B MAs

Mine area	Depth of burial (m)	Elevation From sea level (m)	Methane content (m^3/t)	Expansion pressure (MPa)	Mean permeability coefficient (m^2/MPa^2·d)	Mean borehole flow rate attenuation coefficient (d^{-1})
MA-A	380.21	864.00	23.56	2.82	9.04	0.78
	383.06	865.00	24.56	2.94		
	382.34	865.00	24.99	2.74		
MA-B	443.30	1350.00	13.18	0.87	0.01	0.72
	456.33	1303.00	12.41	0.76		
	511.74	1318.00	13.15	0.92		

are shallower than those in MA-B, the higher methane content and pressure may be attributed to tectonic sealing, higher coal rank, or localised geological features such as fault-controlled accumulation zones. Moreover, historical mining activity and gas migration conditions may have contributed to this disparity.

3.2. Analytical approach to coastal seam pore structure based on fractal theory

This study constructs a fractal permeability model for coal seam (CS) pores based on fractal theory. Considering the combined effects of stress and temperature on the CS, the coal matrix undergoes deformation due to four influencing factors: adsorption, thermal expansion (TE), stress state, and methane [16] -[17]. Accordingly, the stress-induced volume change in the coal matrix is expressed by Eq. (1).

$$\delta_m = \frac{3paRT}{V_0 E_A} \ln \ln \frac{1+bc}{1+bc_0} + \alpha_T \Delta T + \varphi_m - \varphi_{m0} + \frac{\Delta \sigma_m}{B_m} \tag{1}$$

In Eq. (1), p is the density (g/cm^3) of coal rock. a and b are adsorption constant (AC). R is gas constant and T is temperature. V_0 is standard molar volume. E_A is the modulus of expansion from adsorption of coal rock. c and c_0 are gas pressure and gas initial pressure, respectively. α_T is coefficient of TE and ΔT is temperature increase. φ_m is coal matrix porosity and φ_{m0} is the initial coal matrix porosity. $\Delta\sigma_m$ is the effective stress increase amount of coal rock matrix (CRM). B_m is the modulus of rigidity of the CRM. Since coal is a porous medium consisting of CRM and fractures together, the study assumes its isotropy. Under the influence of temperature and stress, the mathematical expressions of the effective stress increase quantity $\Delta\sigma_m$ of the CRM and the porosity change φ_f of the fissures are shown in Eq. (2) [18].

$$\begin{cases} \Delta\sigma_m = \left(\dfrac{3paRT}{V_0 E_A} \ln \dfrac{1+bc}{1+bc_0} + \alpha_T \Delta T + \varphi_m - \varphi_{m0} - \delta_V \right) \left(\dfrac{d_0}{hB_f} + \dfrac{1}{B_m} \right)^{-1} \\ \varphi_f = \varphi_{f0} + \Delta\varphi_f \approx \dfrac{3d_0}{h_0} + \dfrac{3\Delta d_0}{h_0} = \varphi_{f0} \left(1 + \dfrac{\Delta d_0}{d_0} \right) \end{cases} \tag{2}$$

In Eq. (2), δ_V denotes the volumetric stress change of coal under temperature and effective stress. B_f denotes the modulus of rigidity of the coal rock fissure. d_0 denotes the width of the initial cleavage. h denotes the width of the coal matrix. h_0 denotes the width of the initial coal matrix. φ_{f0} denotes the porosity of the initial fissure. $\Delta\varphi_f$ denotes the increase in effective stress of the coal matrix. Δd_0 denotes the increase in initial fracture width. The formula for calculating the coal rock permeability k/k_0 and fractal permeability model k/k_a can be shown in Eq. (3).

$$\begin{cases} \dfrac{k}{k_0} = \left(\dfrac{\varphi_f}{\varphi_{f0}}\right)^3 = \left[1 - \dfrac{3B_m}{\varphi_{f0}B_m + 3B_f}\left(\dfrac{3paRT}{V_0E_A}\ln\dfrac{1+bc}{1+bc_0} + \alpha_T\Delta T + \varphi_m - \varphi_{m0} - \delta_V\right)\right]^3 \\ \dfrac{k}{k_a} = \dfrac{k}{k_0}\left(1 + \dfrac{D}{c}\right) \end{cases} \tag{3}$$

In Eq. (3), D denotes the slip factor. Since coal rock contains a large number of micropores, the slip factor helps correct the theoretical results of coal rock pore characterisation [19]. This study clarifies the pore structure (PS) characterisation method of coal seams (CSs) based on fractal theory. It also utilises the Autosorb iQ 2, a fully automatic gas adsorption analyser manufactured by Quantachrome Company (USA), as the instrument for liquid nitrogen adsorption (NA) analysis of coal seams (CSs). The details are shown in Fig. 2. In Fig. 2(a), the structural pore detection of coal seams (CSs) based on fractal theory is mainly categorised into photoelectric radiation and fluid intrusion methods. Among these, scanning electron microscopy (SEM) and computed tomography (CT) are mainly suitable for small, medium, and large pores, while small-angle X-ray scattering (SAXS) and small-angle neutron scattering (SANS) are primarily used for micropores. Transmission electron microscopy (TEM) is suitable for pores with a pore size (PS) range of 1 nm to 10 μm. The nitrogen adsorption (NA) instrument used for CS testing is shown in Fig. 2(b).

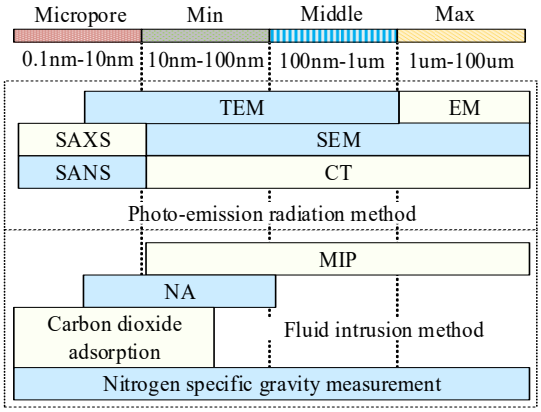

(a) Characterization methods based on fractal theory

(b) Autosorb iQ 2 automatic gas sorption analyzer

Fig. 2. Characterisation of pore structure of coal samples based on fractal theory and selection of testing instruments

This study utilised this instrument to measure the nitrogen isothermal adsorption and desorption curves of CSs. Meanwhile, based on the established fractal permeability model of coal rock, the study sampled the No. 9 CS in MA-A and the No. 20 CS in MA-B. The collected CS samples were processed by crushing and sieving and then divided into two groups based on the collection area for experimentation and analysis. The fractal dimension (FD) of the coal samples was calculated using the Frenkel-Halsey-Hill (FHH) model based on nitrogen adsorption isotherms. The slope of the ln(V) versus ln[ln(P_0/P)] plot in the multilayer adsorption region was used to determine the FD, following standard approaches reported in the literature [Ref.]. This method is commonly applied to evaluate surface and pore complexity in carbonaceous materials.

To ascertain the pore structure (PS), the study relies on the gas adsorption approach due to the complex structure and high pore abundance in CSs. The determination of pore radius n is carried out using the Kelvin equation, as shown in Eq. (4)

$$n = \frac{-0.414}{\ln P / P_0} \tag{4}$$

In Eq. (4), P/P_0 denotes relative pressure (RP). Meanwhile, during the low-temperature NA adsorption of the CSas, the PS of the CSas is detected synchronously by the CO_2 adsorption method and by the Autosorb iQ 2 fully automatic gas adsorption analyser.

3.3. Methods of methane recovery based on fractal theory

To accurately account for the impact of temperature on the adsorption characteristics (AC) of coal, this study first enhances the conventional Langmuir model. A redundant adsorption correction model is introduced to derive the mathematical formula for monolayer adsorption on the outer surface of the coal rock body, as shown in Eq. (5)

$$V_{ex} = a_0 A_0 \cdot \frac{\exp\left(-\frac{\partial}{T} - \frac{E_0}{RT}\right) \cdot c}{1 + b_0 \cdot \exp\left(-\frac{E_0}{RT}\right) \cdot c} (1 - p_g / p_a) \tag{5}$$

In Eq. (5), a_0 and b_0 denote the initial AC A_0 denotes the pre-exponential coefficient. ∂ denotes the coefficient of temperature change on adsorption energy. E_0 denotes the initial adsorption energy. p_g and p_a denote the densities of the free and adsorbed phases, respectively. The pore structure (PS) and surface properties of coal seams (CSs) vary significantly. The adsorption characteristics (AC) of coal rock exhibit variations depending on its equivalent adsorption heat. Therefore, the study investigates the optimization of the mathematical formula for methane adsorption-desorption (MAD) using fractal dimension (FD), as shown in Eq. (6).

$$\begin{cases} S \infty \theta^{(2-D_r)/2} \\ V'_{ex} = a_0 \cdot \theta^{(2-D_r)/2} \cdot A_0 \cdot \dfrac{\exp\left(-\frac{\partial}{T} - \frac{E_0}{RT}\right) \cdot c}{1 + b_0 \cdot \exp\left(-\frac{E_0}{RT}\right) \cdot c} (1 - p_g / p_a) \end{cases} \tag{6}$$

In Eq. (6), S denotes the size of the SSA of the coal rock mass. D_r denotes the FD. θ denotes the effective cross-sectional area of adsorbed molecules. Based on the above equation, the methane adsorption (MAD) isothermal curves for the two types of coal seam samples (CSas) under constant temperature conditions are studied and measured using the experimental apparatus. Subsequently, the effect of coal seam (CS) structure on MAD variation is analysed. The specific experimental apparatus is shown in Fig. 3.

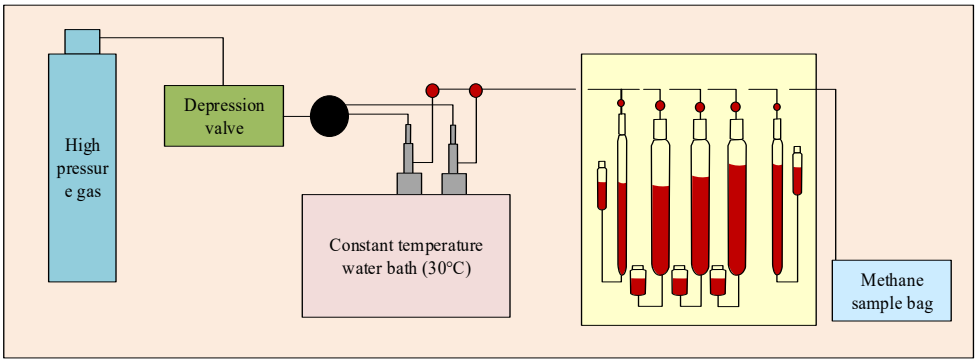

Fig. 3. Flow of methane adsorption experiment

In Fig. 3, the study first prepares and dispenses the CSas. The samples undergo pinhole processing at 60°C for 8 hours and are then flushed with pure methane gas at 5 MPa. Once aerated, the CSas are placed in a thermostatic water bath at 30°C and left to equilibrate for 8 hours. Afterwards, MAD measurements are conducted, along with monitoring changes in ambient pressure and temperature. Based on this setup, the study further performs MDE experiments, as illustrated in Fig. 4.

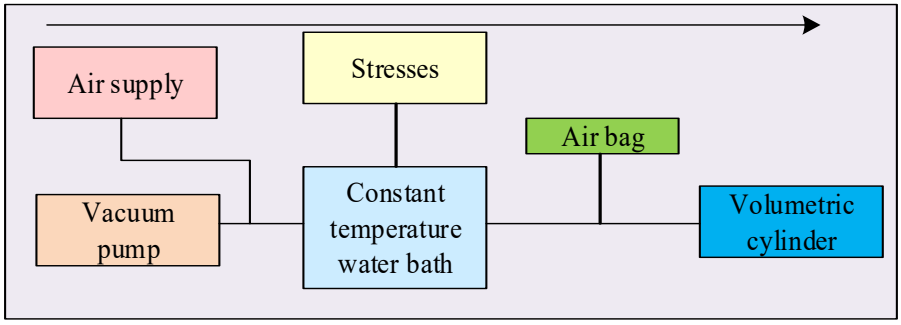

Fig. 4. Methane desorption experimental procedure

In Fig. 4, the pre-treatment steps for CSas remain consistent with those in the MAD experiments. Additionally, the study conducts MDE experiments at five pressure points and employs the drainage method to calculate the drainage volume at each pressure point.

4. Results and discussion

The study first conducts a fractal analysis of the pore structure (PS) of coal seam samples (CSas) from two mining areas (MAs). Next, it examines the methane recovery results, including adsorption and desorption tests of the coal seams (CSs).

4.1. Fractal analysis of CSPS

The analysis begins with an isothermal profile assessment of CS pores from MA-A and MA-B, using an adsorption analyser. Two CSas are collected from the No. 9 CS in MA-A, and two CSas from the No. 20 CS in MA-B. These samples are processed following the procedures outlined in the previous section. The nitrogen adsorption (NA) and desorption isothermal curves of No. 9 CS in MA-A and No. 20 CS in MA-B are presented in Fig. 5.

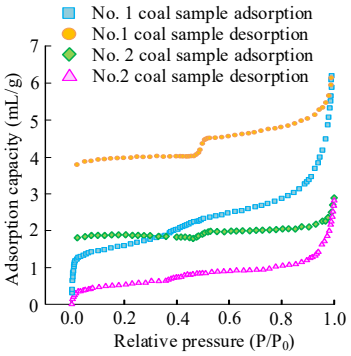

(a) Nitrogen adsorption and desorption isothermal curves of coal samples from A mining area

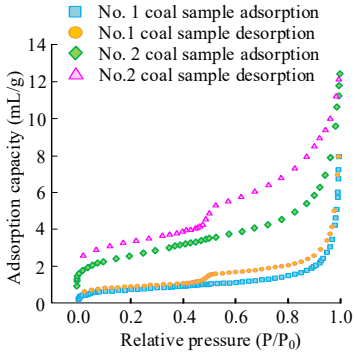

(b) Nitrogen adsorption and desorption isothermal curves of coal samples from B mining area

Fig. 5. Variation of nitrogen adsorption and desorption isothermal curves in the No. 9 seam of the A mine and the No. 20 seam of the B mine

In Fig. 5(a) and (b), the adsorption amounts of the two coal seam samples (CSas) from No. 9 CS in MA-A exhibit significant variation, whereas the difference between the two CSas from No. 20 CS in MA-B is 4.23 mL/g. Compared to MA-A, the nitrogen adsorption (NA) amounts of CSas from MA-B are notably higher.

As the relative pressure (RP) increases, both NA and resolution in CSas from both MAs rise sharply at the initial stage before stabilising. When RP increases from 0.8 P/P_0 to 1.0 P/P_0, the amount of adsorbed and desorbed nitrogen surges again. A comparison of the adsorption and desorption curves of both MAs reveals hysteresis, which is more pronounced in MA-A, indicating a more complex coal seam pore structure (CSPS).

Building on these findings, the study further analyses the CO_2 adsorption and desorption isothermal curves in both MAs, as shown in Fig. 6.

In Fig. 6(a), the CO_2 adsorption amount of the 2nd CSa from No. 9 CS in MA-A is higher than that of the 1st CSa, reaching 28.33 mL/g, while the 1st CSa exhibits a maximum CO_2 adsorption of 27.43 mL/g.

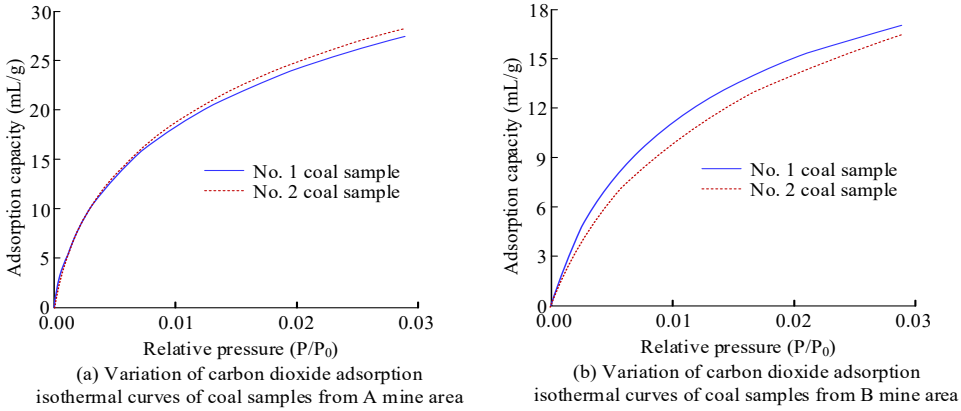

(a) Variation of carbon dioxide adsorption isothermal curves of coal samples from A mine area

(b) Variation of carbon dioxide adsorption isothermal curves of coal samples from B mine area

Fig. 6. CO_2 adsorption and desorption isothermal curves from two mines

As seen in Fig. 6(b), the CO_2 adsorption curves for CSas from both MAs show a direct relationship with the relative pressure (RP)the adsorption increases as RP increases. Additionally, the CO_2 adsorption capacity of CS in MA-A is higher than in MA-B, which may be attributed to its larger pore structure (PS). The PS in coal seams (CSs) provides space for physical adsorption of CO_2, while the oxygen-containing functional groups in coal form strong chemical adsorption bonds with CO_2 molecules, leading to greater adsorption in MA-A.

The adsorption curves of both coal seams transition smoothly and gradually reach saturation with increasing RP, aligning with the modified Langmuir multimolecular layer adsorption model.

To analyse pore structure information (PSi), the study employed a combination of the Dubinin-Radushkevich (D-R) model and the Dubinin-Astakhov (D-A) equation model based on nitrogen and CO_2 adsorption methods. The mesoporous pore volume (Mes-PV) of CSas (0.935 nm) was measured using density functional theory (DFT) combined with NA. Meanwhile, the Barrett-Joyner-Halenda (BJH) method, combined with NA, was used to measure mesoporous and macroporous pore volume (Mac-PV) of CSas (2-300 nm). Additionally, DFT combined with CO_2 adsorption was utilised to measure the microporous pore volume (Mic-PV) of CSas (0.3-1.5 nm). The results are summarised in TABLE 3.

TABLE 3

Pore analysis of coal samples from two mines

Coal sample	Pore size (nm)				Pore volume (mL/g)				
	Nitrogen adsorption		CO_2 adsorption		Microporous 0.3-1.5 nm	Mesoporous 0.9-35 nm	Mesoporous, macroporous 2-300 nm	Total hole capacity	Microporous pore volume (%)
	Average pore size	Fewest pore size	Average pore size	Fewest pore size					
A-No. 1	2.642	1.878	0.866	1.258	0.081	0.007	0.006	0.089	93.258
A-No. 2	2.451	1.822	0.849	1.279	0.088	0.003	0.004	0.092	95.652
B-No. 1	2.108	1.761	0.910	1.301	0.062	0.005	0.008	0.071	87.324
B-No. 2	2.852	1.680	0.933	1.362	0.067	0.008	0.012	0.079	84.810

In TABLE 3, the average PSi of CSas from MA-A ranged from 2.451 to 2.642 nm. The average PSi of CSas from MA-B is between 2.108-2.852 nm. Combining the most available pore diameters of the two MAs, it can be realized that the number of micropores in the CSas is relatively large. The results of pore fusion measurements of CSas from both MAs indicated that the percentage of Mic-PV of CSas from MA-A is above 93%, and the highest percentage of Mic-PV of CSas from MA-B is 87.324%. This indicates that the percentage of Mic-PV of CSas from MA-A is obviously better than that of CSas from MA-B. The Mes-PV and Mac-PV of the CSas from the two MAs were compared, and it was found that the CSas from MA-B accounted for more, which is consistent with the CSs' ability to transport more methane gas. Fig. 7 displays the SSA measurements of the CSas's pores from the two MAs.

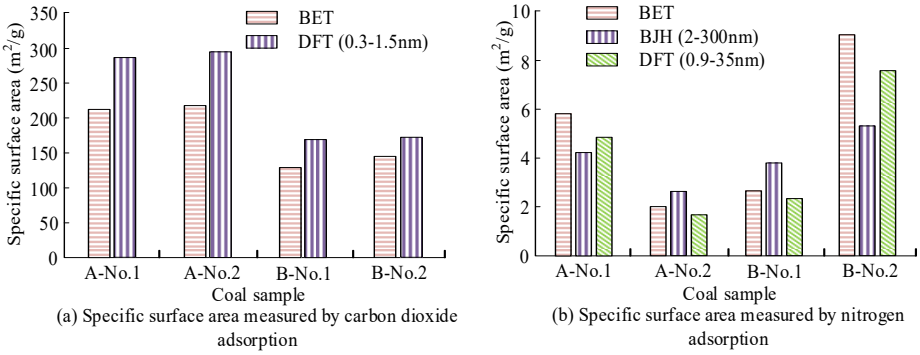

Fig. 7. SSA measurements of the pores of coal samples from two mines

In TABLE 3, the average pore size index (PSi) of CSas from MA-A ranges between 2.451 and 2.642 nm, while for CSas from MA-B, it falls between 2.108 and 2.852 nm. Analysing the dominant pore diameters in both MAs, it is evident that micropores constitute a significant proportion of the CSas' pore structure.

The pore fusion measurements reveal that the microporous pore volume (Mic-PV) of CSas from MA-A exceeds 93%, whereas the highest Mic-PV percentage in CSas from MA-B is 87.324%. This suggests that CSas from MA-A have a higher proportion of micropores compared to CSas from MA-B.

Further comparison of the mesoporous pore volume (Mes-PV) and macroporous pore volume (Mac-PV) between the two MAs indicates that CSas from MA-B contain a higher proportion of Mes-PV and Mac-PV, which correlates with their greater capacity for methane gas transport.

Fig. 7 presents the specific surface area (SSA) measurements of the CSas' pore structures from both mining areas.

In TABLE 4, when the relative pressure (RP) $P/P_0 < 0.45$, the fractal dimensions (FDs) of CSas from both MAs range between 2.51 and 2.67, with a fitting accuracy (R^2) of 0.97 or higher. When RP $P/P_0 > 0.50$, the FDs fall within the range of 2.43-2.75, with a fitting accuracy exceeding 0.98.

Notably, the FD of MA-A is significantly higher than that of MA-B, suggesting that the surface structure of CSas in MA-A is more complex. This increased structural complexity enhances the adsorption capacity of gases such as methane, making MA-A more favorable for gas adsorption.

TABLE 4

Calculated fractal dimensions for the two mines

Coal sample	Relative pressure <0.45		Relative pressure >0.50	
	D_1	R_1	D_2	R_2
A-No.1	2.665	0.974	2.649	0.998
A-No.2	2.666	0.971	2.750	0.989
B-No.1	2.509	0.997	2.637	0.994
B-No.1	2.575	0.989	2.425	0.986

4.2. Regularity analysis of methane recovery

Using the methane adsorption (MAD) and methane desorption (MDE) detection methods, this study further examined the MAD isothermal curves of four CSas collected from the two mining areas. The results are presented in Fig. 8. In Fig. 8, as the pressure increases, the methane adsorption (MAD) amount of the two CSas collected from No. 9 CS in MA-A and No. 20 CS in MA-B also increases. The change curve remains relatively smooth. The difference in MAD amounts between the two samples from No. 9 CS in MA-A is minimal, whereas the MAD amount of the two Csas from No. 20 CS in MA-B shows a significant difference. TABLE 5 presents the adsorption constants a and b of Csas from the two mining areas.

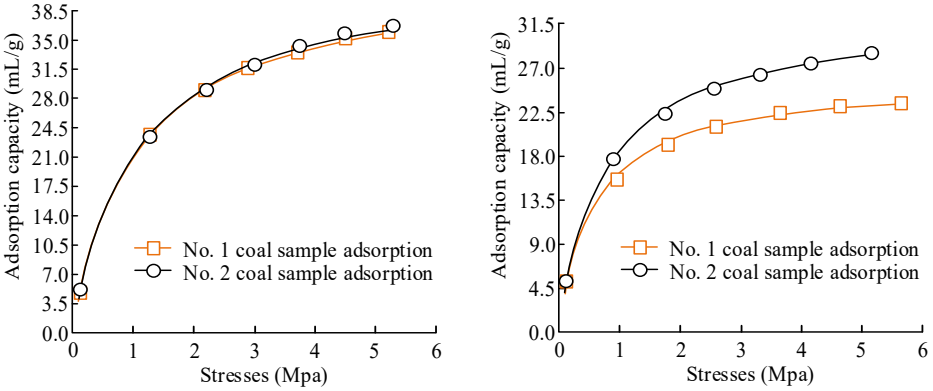

(a) Isothermal adsorption curve of methane in A mine area

(b) Isothermal adsorption curve of methane in B mine area

Fig. 8. Methane isothermal adsorption curves for two mine sites

In TABLE 5, the isothermal adsorption data of adsorption constants (AC) *a* and *b* for the four CSas from the two mines are fitted to the modified Langmuir model with an accuracy of 0.99 or higher. This confirms that the methane adsorption (MAD) detection method used in the study is reliable and valid. The values of AC *a* and *b* for CSas from the two MAs indicate that the AC *a* of MA-A is significantly higher than that of MA-B, suggesting that MA-A has a greater methane adsorption limit and stronger adsorption capacity. However, the AC *a* values of the two CSas from No. 20 CS in MA-B show a large variation, indicating that the 2nd CSa from MA-B

exhibits a significantly higher methane adsorption capacity than the 1st CSa. Building on these findings, and considering the previous pore structure (PS) analysis of CSas, the study further examines the impact of CSPS on MAD. The detailed results are presented in Fig. 9.

TABLE 5

Values of adsorption constants a and b for coal samples from two mines

Coal sample	a (m^3/t)	b (m^3/t)	R^2
A-No.1	36.612	1.563	0.998
A-No.2	37.470	1.502	0.998
B-No.1	21.533	1.579	0.997
B-No.1	28.071	1.692	0.994

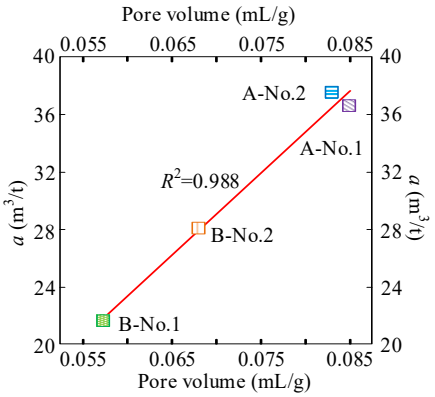

(a) Relationship between the pore volume of coal samples and the limiting adsorption capacity a value

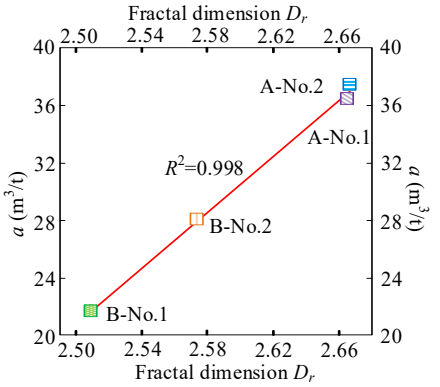

(b) Relationship between the fractal dimension D_r of coal samples and the limiting adsorption capacity a value

Fig. 9. Effect of CSPS on methane adsorption

The relationship between pore volume (PV) and adsorption capacity (AC) for pores smaller than 2 nm in the CSas from both MAs is illustrated in Fig. 9(a). The correlation between PV and AC a in the CSas from the two mines reaches 0.988, indicating a strong positive correlation between pore structure (PS) and methane adsorption (MAD). Similarly, as shown in Fig. 9(b), the relationship between fractal dimension (FD) and MAD constant a for CSas from both MAs demonstrates a correlation as high as 0.998. This suggests that FD has a significant impact on MAD capacity. The observed correlation between fractal dimension (FD) and methane adsorption capacity suggests that samples with more complex pore structures tend to exhibit higher methane adsorption. However, it is acknowledged that this relationship may be indirect. A higher FD often reflects a larger specific surface area (SSA) or a greater proportion of micropores, both of which are independently known to enhance adsorption capacity. To further clarify this, we compared samples with similar SSA but varying FD, and found that differences in MAD were still evident, suggesting a potential independent contribution of FD. Nonetheless, a more robust evaluation using multivariate statistical analysis (e.g., principal component analysis or regression modeling) is recommended in future work to isolate the specific influence of FD from other cor-

related parameters. Moreover, the results indicate that CSas with a more complex pore surface and higher FD exhibit superior methane adsorption capacity. Building on the pore structure (PS) characteristics analysed in the previous section, the study further investigates the methane adsorption limit volume of CSas collected from both mines. The detailed results are presented in Fig. 10.

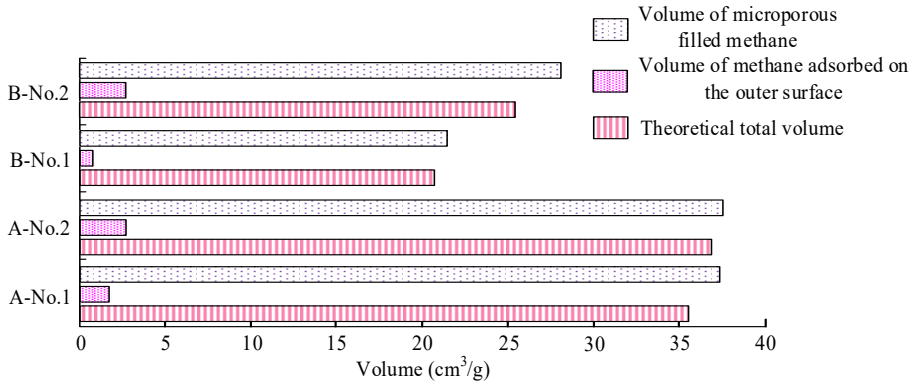

Fig. 10. Volume of methane adsorbed at the limit of coal samples taken from two mines

In Fig. 10, the micropore-filled methane volumes for the two CSas from MA-A are 35.53 cm^3/g and 36.89 cm^3/g, accounting for 95.28% and 98.43% of the total theoretical volume, respectively. Similarly, the micropore-filled methane volumes for the two CSas from MA-B are 20.74 cm^3/g and 25.45 cm^3/g, making up 96.30% and 90.43% of the total theoretical volume, respectively. A comparison between the volume of methane adsorbed on the outer surface of the CSs and the methane-filled micropore volume reveals that the majority of the expansion energy of methane and other gases in the CSas is dispersed within the pore structure (PS) of the CS.

5. Conclusion

To investigate the impact of coal seam pore structure (CSPS) on methane gas expansion energy and methane recovery efficiency, this study applied fractal theory analytical methods alongside practical experiments to analyse the CSPS in depth. The findings revealed that the microporous pore volume (Mic-PV) percentage in the coal seams (CS) of both mining areas (MAs) ranged from 84.810% to 95.652%. When the relative pressure (RP) P/P_0 exceeded 0.50, the fractal dimension (FD) of the two MAs ranged between 2.43 and 2.75, indicating a positive correlation between pore complexity and methane adsorption capacity (MAD) with higher FD values leading to stronger methane adsorption.

By comparing CSas from MA-A and MA-B, it was observed that MA-A exhibited a higher Mic-PV percentage and specific surface area (SSA), resulting in superior MAD performance. Furthermore, optimising CSPS was found to significantly enhance methane recovery efficiency, which is crucial for both coal mine safety and the efficient utilisation of coalbed methane (CBM) resources.

However, some limitations remain in establishing a comprehensive relationship between CSPS and methane recovery, particularly in terms of experimental condition control and the representativeness of CSas samples. Future research should extend CSPS analysis to more coal mines under varying geological conditions to improve the generalisability and applicability of the findings. Additionally, exploring new CSPS optimisation techniques could further enhance methane recovery efficiency and coal mine safety.

Rerefences

[1] F. XU et al., The status and development strategy of coalbed methane industry in China. Pet. Explor. Dev. **50**, 4, 765-783 (2023).
DOI: https://doi.org/10.1016/S1876-3804(23)60427-6

[2] N. Kursunoglu, Fuzzy multi-criteria decision-making framework for controlling methane explosions in coal mines. Environ. Sci. Pollut. Res. **31**, 6, 9045-9061 (2024).
DOI: https://doi.org/10.1007/S11356-023-31782-0/tables/12

[3] R. Zhang, S. Liu, L. He, T.P. Blach, Y. Wang, Characterizing Anisotropic Pore Structure and Its Impact on Gas Storage and Transport in Coalbed Methane and Shale Gas Reservoirs. Energy and Fuels **34**, 3, 3161-3172 (2020).
DOI: https://doi.org/10.1021/acs.energyfuels.0c00109

[4] J. Linghu et al., Influence of deep magma-induced thermal effects on the regional gas outburst risk of coal seams. Int. J. Coal Sci. Technol. **8**, 6, 1411-1422 (2021).
DOI: https://doi.org/10.1007/s40789-021-00452-2/figures/13

[5] M. Khan et al., Extracting and Predicting Rock Mechanical Behavior Based on Microseismic Spatio-temporal Response in an Ultra-thick Coal Seam Mine. Rock Mech. Rock Eng. **56**, 5, 3725-3754 (2023).
DOI: https://doi.org/10.1007/S00603-023-03247-W

[6] Y. Li, W. Liu, D. Song, Z. Ren, H. Wang, X. Guo, Full-scale pore characteristics in coal and their influence on the adsorption capacity of coalbed methane. Environ. Sci. Pollut. Res. Int. **30**, 28, 72187-72206 (2023).
DOI: https://doi.org/10.1007/S11356-023-27298-2.

[7] Z. J. MA Dan, LI Qiang, Pore structure characterization and nonlinear seepage characteristics of rock mass in fault fracture zones. J. China Coal Soc. **48**, 666-676 (2023). Accessed: Mar. 29.2025. [Online].
Available: https://www.mtxb.com.cn/en/article/id/5dbcf7d6-2de2-4e4a-8eeb-7bb8294a9b33

[8] Y. Yuan, F. Cai, L. Yang, Pore structure characteristics and fractal structure evaluation of medium- and high-rank coal. Energy Explor. Exploit. **40**, 1, 328-342 (2022).
DOI: https://doi.org/10.1177/01445987211034315/asset/16d79eee-86e5-4245-b6b5-c59f44a37208/assets/images/large/10.1177_01445987211034315-fig6.jpg

[9] M. Razavifar et al., Rock Porous Structure Characterization: A Critical Assessment of Various State-of-the-Art Techniques. Transp. Porous Media **136**, 2, 431-456 (2021).
DOI: https://doi.org/10.1007/S11242-020-01518-6

[10] C. Li, H. Yao, C. Xin, H. Li, J. Guan, Y. Liu, Changes in Pore Structure and Permeability of Middle-High Rank Coal Subjected to Liquid Nitrogen Freeze-Thaw. Energy and Fuels **35**, 1, 226-236 (2021).
DOI: https://doi.org/10.1021/acs.energyfuels.0c02294

[11] W. Choi, Y. Lee, J. Mok, Y. Seo, Influence of Competitive Inclusion of CO2 and N2 on sII Hydrate-Flue Gas Replacement for Energy Recovery and CO2 Sequestration. Environ. Sci. Technol. **54**, 12, 7562-7569 (2020).
DOI: https://doi.org/10.1021/acs.est.0c00583

[12] J.S. Pandey, C. Karantonidis, Q. Ouyang, N. Von Solms, Cyclic Depressurization-Driven Enhanced CH4Recovery after CH4-CO2Hydrate Swapping. Energy and Fuels **35**, 11, 9521-9537 (2021).
DOI: https://doi.org/10.1021/acs.energyfuels.1c00685/suppl_file/ef1c00685_si_003.mp4

[13] Y. Zhou, Y. Liu, Y. Shi, Y. Zhang, J. Shi, P. Sun, Strategies for heat recovery in a reverse flow reactor designed to lessen coal mine methane emissions test. Energy Sources, Part A Recover. Util. Environ. Eff. **45**, 3, 8665-8685 (2023). DOI: https://doi.org/10.1080/15567036.2023.2230941

[14] B. Li et al., Effects of Liquid CO2 Phase Transition Fracturing on Methane Desorption of Coal. Energy and Fuels **38**, 6, 5088-5097 (2024).
DOI: https://doi.org/10.1021/acs.energyfuels.3c04707

[15] A.M. Ali, M.Y. Kwaya, A. Mijinyawa, A.A. Aminu, Z.M. Usman, Molecular dynamics and energy distribution of methane gas adsorption in shales. J. Nat. Gas Geosci. **8**, 1, 1-15 (2023).
DOI: https://doi.org/10.1016/j.jnggs.2022.12.004

[16] B. Wang et al., Combined Effects of Stress, Gas Adsorption, and Temperature on the Evolution of Coal Seam Permeability and Slippage Effect. ACS Omega **8**, 42, 39376-39389 (2023).
DOI: https://doi.org/10.1021/acsomega.3c05001/asset/images/large/ao3c05001_0020.jpeg

[17] X. Su, Z. Feng, Y. Cheng, T. Cai, Y. Shen, Thermal Expansion and Adsorption Characteristics of Coal Based on Temperature Change and Its Influence on the Slippage Effect. Energy and Fuels **37**, 9, 6558-6568 (2023).
DOI: https://doi.org/10.1021/acs.energyfuels.3c00513

[18] C. Fan, X. Jiang, N. Fan, B. Xiao, L. Yang, Z. Yang, Scale Effect of Coal Porosity and Permeability Characteristics Based on CT 3D Reconstruction from a Microperspective. Energy and Fuels **38**, 3, 1813-1821 (2024).
DOI: https://doi.org/10.1021/acs.energyfuels.3c04359

[19] H. Xu et al., Quantitative Study of the Effects of Pore Structure and Wettability on the Water Spontaneous Imbibition Behaviors in Coal. Energy and Fuels **38**, 1, 184-199 (2024).
DOI: https://doi.org/10.1021/acs.energyfuels.3c04104